Electrochimica Acta 352 (2020) 136483

Contents lists available at ScienceDirect

Electrochimica Acta

journal homepage: www.elsevier.com/locate/electacta

The electrochemical behavior of 4-nitrobenzyl bromide and its catalytic activity for reduction of CO_2 in the acetonitrile solvent at the Cu/Pd/rGO/GCE surface

Safoora Mohammadzadeh , Hamid R. Zare *, Hossein Khoshro , Kobra Ghobadi , Ali Benvidi

Department of Chemistry, Yazd University, Yazd, 89195-741, Iran

ARTICLE INFO

Article history:
Received 28 January 2020
Received in revised form
12 May 2020
Accepted 13 May 2020
Available online 26 May 2020

Keywords:
Carbon dioxide
4-Nitrobenzyl bromide
4-Nitrophenylacetate
Catalytic activity
Cu and Pd nanoparticles

ABSTRACT

In this study, 4-nitrobenzyl bromide was used as a catalyst for reduction of CO_2 and as an initial substrate for electrosynthesis of 4-nitrophenylacetic acid. Cu nanoparticles/Pd nanoparticles/reduced graphene oxide nanocomposite modified glassy carbon electrode (Cu/Pd/rGO/GCE) was used to promote electroactivation of CO_2. rGO film was fabricated via electrochemical reduction of dispersed GO nanosheets on the GCE surface. Cyclic voltammetry procedure was applied in two steps to deposit Pd and Cu nanoparticles on the rGO/GCE surface. The morphology and structure of the nanocomposites were characterized using FESEM, EDS, AFM and XRD analysis. FTIR, ^{1}H and ^{13}C NMR spectral characteristics were used to identify the final products of the catalytic process. The electrocarboxylation of 4-nitrobenzyl bromide occurs at a potential which is less negative than those reported for other aryl halides. The results indicate that 4-nitrobenzyl bromide, as a catalyst, plays a dual role in the electrosynthesis of 4-nitrophenylacetate. The dual role includes the electrocatalytic reduction of CO_2 and reaction of produced $CO_2^{\bullet-}$ with 4-nitrobenzyl bromide radical anion. Finally, an EC'C mechanism is proposed for the electrosynthesis of 4-nitrophenylacetate.

1. Introduction

Carbon dioxide (CO_2) is considered as part of the carbon cycle in the Earth's system [1]. Fossil fuel combustion as dominant source of anthropogenic emissions of CO_2 to the atmosphere had been introduced [2]. Synthesis of organic compounds using CO_2 as one of the initial materials, not only helps to decrease the concentration of CO_2 in the atmosphere but also exploits it as a low-cost source of carbon [3]. Due to the inertness and low activity of CO_2, its activation is first step for synthesis of organic compounds. Different techniques of CO_2 activation such as chemical reduction by metals [4], thermochemical conversion [5], radiochemical method [6], photochemical conversion [7], biochemical conversion [8], bioelectrochemical conversion [9], photoelectrochemical conversion [10,11] and electrochemical conversion [12–15] have been applied. Among various possible approaches, CO_2 electrochemical reduction is a suitable way for conversion of CO_2 under mild conditions [16]. A number of organic compounds [17,18] and transition metal complexes [19–21] were used for electrocatalytic reduction of CO_2. When an electrocatalyst is used for reduction of CO_2, there are some challenges such as difficulty of separating the electrocatalyst at the end of electrosynthesis and some possible unwanted reactions that lead to form intermediates which cause electrocatalyst deactivation [22]. Application of electroactive compounds which are able to fulfill a double duty, namely the electrocatalytic reduction of CO_2 to $CO_2^{\bullet-}$ and reaction with the created $CO_2^{\bullet-}$ to produce a product, can make a major contribution to resolving this problem. There are some reports regarding the electrochemical reduction of 4-nitrobenzyl halides [23,24]. In these reports, the nitro functional group in 4-nitrobenzyl halides serves as an intramolecular component in the cleavage of carbon halogen bonds [23,24]. Bond breaking can provide a suitable site for substitution reactions, which leads to replacement of halogen ions with a radical species.

On this basis, the present study demonstrates that 4-nitrobenzyl bromide, as a redox catalyst, has a dual activity including 1) the catalytic reduction of CO_2 and 2) the chemical reaction of the

* Corresponding author.
E-mail address: hrzare@yazd.ac.ir (H.R. Zare).

https://doi.org/10.1016/j.electacta.2020.136483
0013-4686/

reduced form of 4-nitrobenzyl bromide with $CO_2^{\bullet -}$ to form 4-nitrophenylacetate. It is to be noted that 4-nitrophenylacetate derivatives have been widely used as a mediator in the synthesis of different medicines such as antitumor agents [25] and deprotecting reagents [26]. To improve the performance of 4-nitrobenzyl bromide electrocatalyst toward the reduction of CO_2, a new nanocomposite of Cu nanoparticles/Pd nanoparticles/reduced graphene oxide (Cu/Pd/rGO) was prepared via the simple electrodeposition methods on the GCE surface. rGO is considered as support catalyst [27,28] because of its unique structure and properties, high specific surface area, high electrical conductivity, great mechanical stability, ease of preparation, low cost [29,30] and strong nanoparticle anchoring [28,31]. Direct electrochemical reduction of graphene oxide (GO) to rGO on the electrode surface is faster, more environmentally friendly, and easier to control [32,33] than using reducing agents such as hydrazine [34,35], sodium borohydride [36] and ascorbic acid [37]. Applying composites of graphene–metal nanoparticles have attracted extensive attention which is due to their enhance electron conductivity, high surface area, catalytic properties and good biocompatibility [38–40]. Researchers have reported that Pd and graphene bind strongly because of generated interaction states and transmission channels between them [41–43]. In other words, GO sheets act as scaffolds to grow and anchor Pd nanoparticles (PdNPs) [44]. Because of some attractive properties such as good electrical conductivity and catalytic properties of copper nanoparticles (CuNPs) [45], it was also used for electrode modification. In other words, CuNPs/PdNPs/rGO modified GCE (Cu/Pd/rGO/GCE) was used for electrocatalytic reduction of CO_2 by 4-nitrobenzyl bromide. Objective of this paper is to present the performance of 4-nitrobenzyl bromide, as an excellent mediator, for electrocatalytic reduction of CO_2 at the Cu/Pd/rGO nanocomposite modified electrode surface.

2. Experimental

2.1. Chemicals and apparatus

4-Nitrobenzyl bromide (99%), tetrabuthyl ammonium perchlorate (TBAP) (>98.0%), potassium tetrachloro palladate (II) (98%), copper (II) sulphate (99%), acetonitrile solvent (ACN) (99.9%) were purchased from Merck Company. Acetonitrile (ACN) were purified according Ref [46]. ACN was treated with heated neutral $A1_2O_3$ at 600 °C under vacuum (3 h) and then was passed through molecular sieves 4 Å (B.D.H.). The obtained solvent was distilled under N_2 flux at pressure of 4–5 Torr and finally was collected over P_2O_5. TBAP recrystallized from an ethanol solution and was dried under vacuum at 60 °C [46,47]. A phosphate buffer (pH 5) was prepared with 0.1 M H_3PO_4 and 2.0 M NaOH. GO was prepared based on the modified Hummers' method [48]. Gases of CO_2 and Ar had a purity of 99.995%. All the measurements were performed at room temperature. Cyclic voltammetry was carried out using an EG&G PARSTAT 2273 equipped with a Power Suite software program in a conventional three-electrode electrochemical cell containing bare and various modified GCE with a diameter of 2 mm as the working electrode, Ag/AgCl/KCl (sat'd) as the reference electrode, and a Pt wire as the counter electrode. A SAMA 500 electroanalyzer was used for constant potential coulometry (CPC) experiments. Divided and undivided glass cells were used in the electrolysis and voltammetric experiments, respectively. The cells were equipped each with a gas inlet and outlet, a graphite rod as the cathode, an Ag/AgCl/KCl (sat'd) electrode as the reference and a platinum plate (ca.5 cm^2) as the anode. Acetonitrile and TBAP were used as a solvent and a supporting electrolyte respectively. Surface morphologies were analyzed with high-resolution field emission scanning electron microscopy (FESEM), model MIRA3TESCAN-XMU. The morphology of the modified electrodes was determined by atomic force microscope (AFM) images (Nanosurf, Switzerland) and X-ray powder diffraction (XRD) patterns were taken in reflection mode CuKα (λ = 1.5406 Å) radiation in the 2θ range from 10° to 80° on a senware AW-DX300 X-ray diffractometer. Electrochemical impedance spectroscopy (EIS) tests were conducted at a steady-state potential. An AC amplitude potential of 10 mV superimposed on a DC potential was applied, and a frequency span of 100 KHz down to 10 mHz was scanned. The Nyquist plots of impedance data were analyzed using ZsimpWin software.

^1H and ^{13}C NMR were measured on a DRX-400 (Bruker) spectrometer with $CDCl_3$ as a solvent in the presence of $SiMe_4$ as an internal standard. Fourier transform infrared (FTIR) spectrum analysis was performed on an EQUINOX55 spectrometer.

2.2. Preparation of Cu/Pd/rGO/GCE

Prior to modification, the GCE surface was polished with a 0.05 μm alumina slurry on a polishing cloth. The polished electrode was washed with double distilled water and sonicated for a few minutes. For preparation of rGO modified GCE (rGO/GCE), 10.0 μL homogeneous suspension of GO (1 mg mL^{-1}) was dropped on the polished GCE surface and dried in air to form GO/GCE, then it was placed in a phosphate buffer (pH 5) to be reduced electrochemically in the potential range of 0.5 V to −1.5 V and at potential scan rate of 100.0 mV s^{-1}. Finally, it was then washed and dried [32,33,49]. Next, Pd nanoparticles are electrochemically deposited on rGO/GCE surface [50]. The electrode was immersed into a 0.5 M H_2SO_4 solution containing 1.0×10^{-3} M potassium tetrachloro palladate (II), and a repetitive potential scan carried out between 1.2 V and −0.25 V with scan rate of 100 mV s^{-1} for seven cycles. Then, produced Pd/rGO/GCE was rinsed with deionized water. To prepare Cu/Pd/rGO/GCE, electrodeposition method was used easily in sulphuric acid solution (pH 1.5) containing 0.025 M copper sulphate by consecutive cyclic voltammetry (30 scans) in the potential range of 0.5 V to −0.6 V and at scan rate of 100 mV s^{-1} [51].

2.3. Electrolysis procedure

All the electrolysis experiments were performed at constant potential coulometry (CPC) in 50.0 ml of ACN solution containing 0.05 M TBAP. Before each experiment, a definite amount of 4-nitrobenzyl bromide was added to the solution, and Ar gas was bubbled for 20 min. During the electrolysis, consumption of the initial compound, i.e. 4-nitrobenzyl bromide, was followed by TLC tests of aliquots withdrawn from the reaction mixture. In the TLC tests, the spots were identified by irradiation of ultraviolet light. At the end of the electrolysis, 5.0 mL of 0.5 M HCl was added to the solution, and it was stirred for 30 min at room-temperature. Afterwards, the solvent was evaporated, and the residue was separated with a silica gel column under gradient elution. The result of the 4-nitrobenzyl bromide electrolysis in the absence of CO_2 (under an Ar flow) and at the constant potential of −0.89 V showed consumption of about 1.1 F mol^{-1}. Under these conditions, the Faradaic yield in the bare GCE and various modified electrodes surface is about 91%. Also, the ^1H NMR spectral characteristics of the product were as follows: δ 3.09 ppm (s, 4H), δ 7.55 ppm (d.d, 4H, j = 3.2), δ 7.72 ppm (d.d, 4H, j = 3.2) which are related to 1,2-bis(4-nitrophenyl) ethane compound (Fig. S1). The approximate yield of this product at the surface of various electrodes was reported in Table 1. The electrolysis of 4-nitrobenzyl bromide under bubbling of CO_2 at the potential of −0.80 V consumed about 2.04 F mol^{-1}. In the presence of CO_2, the Faradaic yield at the bare GCE and the various modified electrodes surface is about 98%. Final products in the presence of CO_2 were 4-nitrophenylacetate and oxalate as the main

Table 1
The yield of products obtained by the electrolysis of 4-nitrobenzylbromide in the absence of CO_2 (under an Ar flow) and in the presence of CO_2 at the different modified electrode surfaces.

Electrode type[a]	Yield of 1,2-bis(4-nitrophenyl) ethane product in the absence of CO_2	Yield of nitrophenylacetate product in the presence of CO_2	Yield of oxalate product in the presence of CO_2
Bare GCE	85%	73%	27%
rGO/GCE	84%	75%	25%
Pd/rGO/GCE	86%	74%	26%
Cu/Pd/rGO/GCE	87%	76%	24%

[a] GCE: Glassy carbon electrode; rGO/GCE: Reduced graphene oxide/glassy carbon electrode; Pd/rGO/GCE: Pd nanoparticles/reduced graphene oxide/glassy carbon electrode; Cu/Pd/rGO/GCE: Cu nanoparticles/Pd nanoparticles/reduced graphene oxide/glassy carbon electrode.

and the side products, respectively. The approximate yield of each product in the presence of CO_2 at the different electrode surfaces is also reported in Table 1. To make the product easier to separate from the supporting electrolyte salt, at the end of the electrolysis, 5.0 mL of 0.5 M HCl was added to the solution to form 4-nitrophenylacetic acid and oxalic acid. Then, the molecular forms of the products were separated with a silica gel column. The spectral characteristics of the separated product (4-nitrophenylacetic acid) were as follows: FTIR: 3385 cm^{-1} (O–H), 2961 cm^{-1} (–C–H), 2875 cm^{-1} (=C–H), 1727 cm^{-1} (C=O), 1346,1518 cm^{-1} (–N=O), 1095 cm^{-1} (C–O) (Fig. S2). ^{1}H NMR: δ 3.82 ppm (s, 2H), δ 7.47 ppm (d, 2H, j = 6.8), δ 8.17 ppm (d, 2H, j = 6.8), and a wide peak ≈ δ 9.12 ppm (s, 1H) (Fig. S3), ^{13}C NMR: δ 29.67, 123.67, 130.58, 141.09, 147.21, 174.33 ppm (Fig S4). Oxalic acid: FTIR: 3482 & 3443 cm^{-1} (O–H), 1695 cm^{-1} (C=O), 1128 and 1254 cm^{-1} (C–O) (Fig. S5).

3. Results and discussion

3.1. Characterization

The morphology of synthesized Pd nanoparticles (Pd/rGO) and Cu nanoparticles/Pd nanoparticles/reduced graphene oxide (Cu/Pd/rGO) composites were examined by FE-SEM. Figs. 1A and B shows the images with different magnifications of Pd/rGO composite. As can be seen, Pd nanoparticles (PdNPs) have been uniformly deposited on the surface of rGO sheets. Also, FE-SEM images of different magnifications Cu nanoparticles (CuNPs) which are electrodeposited on the Pd/rGO composite surface, (Cu/Pd/rGO), are shown in Figs. 1C and D. It can be seen; the nanoparticles were more densely aggregated. Fig. S6 represents the corresponding energy dispersive spectra (EDS) and elemental mapping images of the synthesized Pd/rGO and Cu/Pd/rGO composites. These data confirm the presence of C, O, Pd and C, O, Pd, Cu elements in the prepared Pd/rGO (Figs. S6A and S6B) and Cu/Pd/rGO (Figs. S6C and S6D) composites, respectively.

The morphology of the rGO/GCE, Pd/rGO/GCE and Cu/Pd/rGO/GCE surface was examined by means of atomic force microscopy (AFM). Figs. 2A–F exhibit 2D and 3D AFM images of the rGO/GCE, Pd/rGO/GCE and Cu/Pd/rGO/GCE, respectively. Figs. 2A and B show that the rGO sheets have a height of about 1.3 μm. After loading PdNPs and CuNPs onto the rGO sheets, height of the Pd/rGO/GCE (Figs. 2C and D) and Cu/Pd/rGO/GCE (Figs. 2E and F) decreased compared to rGO/GCE. The results indicate that the distribution of nanoparticles on the rGO sheets covers rGO's pores and therefore decrease the height of Pd/rGO/GCE and Cu/Pd/rGO/GCE compared to rGO. The XRD pattern of Cu/Pd/rGO/GC electrode was shown in Fig. 3. Three diffraction peaks at 2θ = 38.1, 46.15 and 64.65 are related to Pd (JCPDS No. 00-005-0681). As shown in this figure, obtained crystallographic parameters from the XRD data at 2θ = 43.3, 50.9 and 74.2 are in accordance with crystallographic planes of Cu (JCPDS No. 00-004-0836). The broad peak at around 25° is attributed to the (002) planes of RGO [52].

The active surface area of the different modified electrodes (rGO/GCE, Pd/rGO/GCE and Cu/Pd/rGO/GCE) were estimated using cyclic voltammograms of $K_4Fe(CN)_6$ solution (1.0 mM) at different scan rates. On the basis of Randles- Sevcik equation [53], the effective surface area of rGO/GCE, Pd/rGO/GCE and Cu/Pd/rGO/GCE were obtained 0.038, 0.042 and 0.044 cm^2 respectively.

The geometric area of the bare GCE was 0.0314 cm^2. So, the results indicate that presence of rGO, PdNPs and CuNPs increase the effective surface area of the modified electrodes.

3.2. Electrochemical behavior of 4-nitrobenzyl bromide

The electrochemical behavior of 4-nitrobenzyl bromide ($BrCH_2ArNO_2$) was studied in an ACN solution containing TBAP at the bare GCE, rGO/GCE, Pd/rGO/GCE and Cu/Pd/rGO/GCE surfaces at room temperature by cyclic voltammetry. Fig. 4, voltammogram (a), shows the response of an ACN solution in the absence of 4-nitrobenzyl bromide after being bubbled with Ar gas for 20 min and in the potential range of −0.5 V to −2.2 V at the bare GCE surface. As shown in voltammogram (a), there was no redox peak at the scan rate of 100 mV s^{-1}. Voltammogram (b) shows the response of an ACN solution in the presence of 1.0 mM 4-nitrobenzyl bromide after removing O_2 and CO_2 and in the potential range of −0.50 V to −1.45 V at the bare GCE surface. An irreversible reduction peak (peak I with $E_{pc} = -0.89$ V) and a quasi-reversible redox couple (cathodic peak (II) with $E_{pc} = -1.22$ V and anodic peak (III) with $E_{pa} = -1.07$ V) were appeared. Reduction peak (I) is related to the reduction of the nitro group of 4-nitrobenzyl bromide [23]. One-electron reduction of 4-nitrobenzyl bromide leads to carbon-halogen bond breaking [23]. The process involves an intramolecular electron transfer from the nitro group to the carbon-halogen bond. Subsequently, a dimerized product, 1,2-bis(4-nitrophenyl) ethane, is formed by simultaneous loss of two bromide ions [47,54]. Redox couple (II)/(III) can be attributed to the reduction and oxidation of the dimerized product, i.e. 1,2-bis(4-nitrophenyl) ethane [23]. The result of the electrolysis under an Ar flow and at the constant potential of −0.89 V showed consumption of 1.1 F mol^{-1}. Also, the ^{1}H NMR spectral characteristics of the electrolysis product (Fig. S1) confirm the formation of 1,2-bis(4-nitrophenyl) ethane compound.

In this study, the effect of rGO, PdNPs and CuNPs on the electroreduction of 4-nitrobenzyl bromide was also investigated. Fig. 5 shows the cyclic voltammograms of a bare GCE (voltammogram a), rGO/GCE (voltammogram b), Pd/rGO/GCE (voltammogram c) and Cu/Pd/rGO/GCE (voltammogram d) in an ACN solution containing 1.0 mM 4-nitrobenzyl bromide after removing O_2 (bubbled with Ar gas for 20 min) in the potential range of −0.50 to −1.45 V, respectively. During the transition from the voltammogram (a) to voltammogram (d), it is observed that the peak potential I is shifted

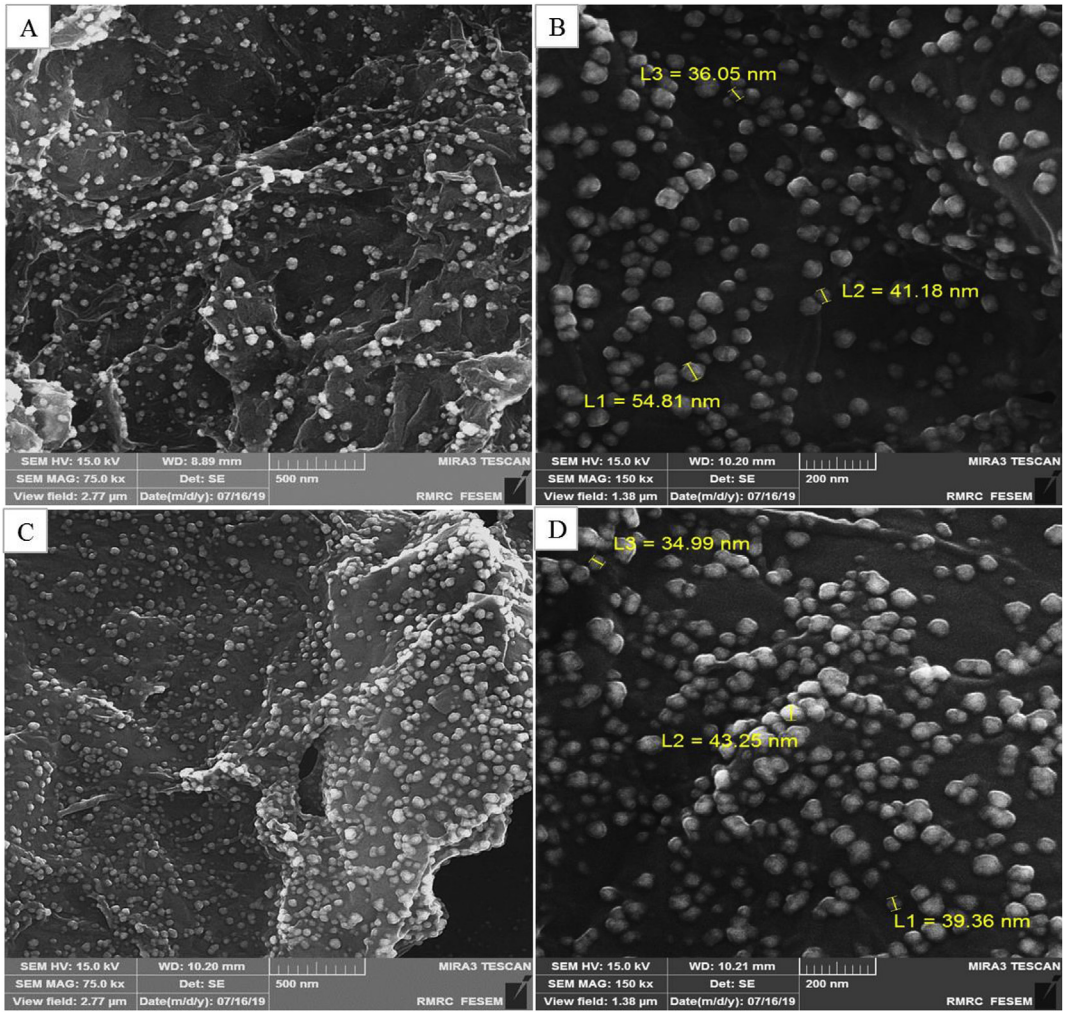

Fig. 1. The FE-SEM images of (A and B) Pd nanoparticles/reduced graphene oxide composite (Pd/rGO) and (C and D) Cu nanoparticles/Pd nanoparticles/reduced graphene oxide composite (Cu/Pd/rGO) with different magnification.

towards less negative values, which is good from the thermodynamically point of view. On the other hand, peak I becomes larger from (a) to (d), which means that the process on the Cu/Pd/rGO/GCE is kinetically faster than the precedents (d > c > b > a). The increase in reduction current obtained with rGO is attributed to its high electrical conductivity [29]. The higher reduction current at the less negative potential (peak I, $E_{pc} = -0.82$ V) at Pd/rGO/GCE can be ascribed to its higher surface area and successive incorporation of PdNPs and rGO in the composite which used for electroreduction of 4-nitrobenzyl bromide. Further investigation of the electrochemical behavior of 4-nitrobenzyl bromide at the Cu/Pd/rGO/GCE surface was performed. According to the obtained results, the reduction of 4-nitrobenzyl bromide at the Cu/Pd/rGO/GCE surface (voltammogram d) occurs at less negative potential (peak I, $E_{pc} = -0.76$ V) in comparison with Pd/rGO/GCE (voltammogram c). Cyclic voltammograms of 4-nitrobenzyl bromide (voltammogram a) and 1.0 mM 1,2-bis(4-nitrophenyl) ethane (product of 4-nitrobenzyl bromide electrolysis) after removing O_2 (bubbled with Ar gas for 20 min), in the potential range of −0.5 V to −1.45 V at the surface of a bare GCE are shown in Fig. 6. These voltammograms are similar those reported in the literature [23]. Spectral characteristics of the electrolysis product (Fig. S1) and above results confirm that the main product of 4-nitrobenzyl bromide electrolysis after removing O_2 is 1,2-bis(4-nitrophenyl) ethane compound.

In addition, consecutive cycles of Cu/Pd/rGO/GC electrode were recorded in ACN solution (0.1 M TBAP) containing 4-nitrobenzyl bromide (not shown). The results indicate that the modified electrode has good stability. Also, the Nyquist plots obtained for the bare GCE and modified GCEs (Fig. 7). Electrochemical impedance spectroscopy (EIS) experiments give the information of impedance changes of bare GCE, rGO/GCE, Pd/rGO/GCE and Cu/Pd/rGO/GCE. EIS of the bare GCE shows highest semicircular and charge transfer resistance ($R_{ct} = 1820.88$ KΩ) (Fig. 7). A comparison of EIS of rGO/GCE and GCE exhibits decreasing radius of semicircular ($R_{ct} = 1382.72$KΩ) that is attributed to high specific surface area and high electrical conductivity of rGO. Also, Fig. 7 shows that electrodeposition of PdNPs on the rGO sheets (Pd/rGO/GCE) leads to a further decrease in R_{ct} (910.05 KΩ). Finally, CuNPs electrodeposited on Pd/rGO/GC surface resulted in decreased of Cu/Pd/rGO/GC charge transfer resistance ($R_{ct} = 760.10$ KΩ).

3.3. Electrochemical activation of CO_2 by 4-nitrobenzyl bromide at the Cu/Pd/rGO/GCE surface

The electrochemical behavior of 4-nitrobenzyl bromide and CO_2 was investigated at the bare GCE, rGO/GCE, Pd/rGO/GCE and Cu/Pd/rGO/GCE surface in an ACN solution containing TBAP at room

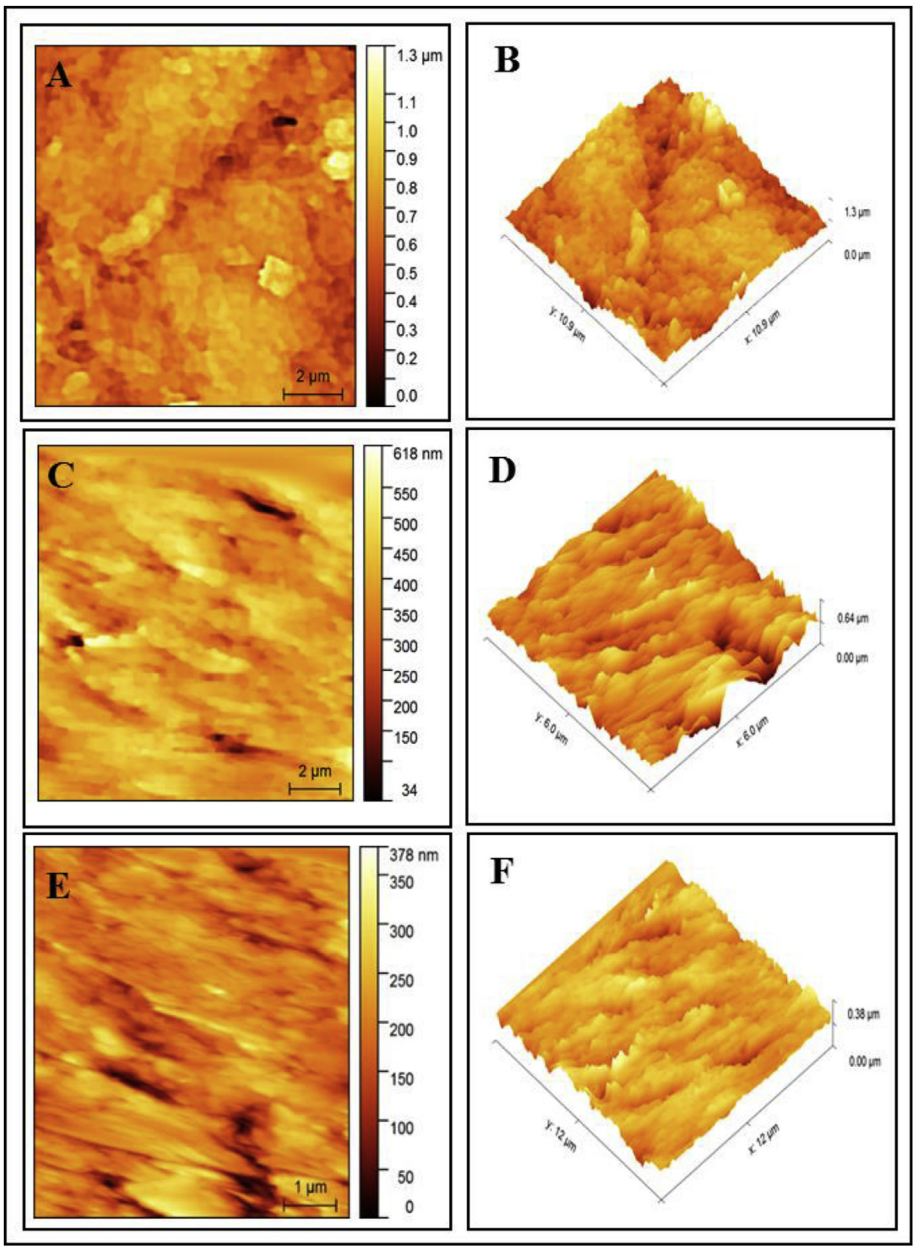

Fig. 2. (A) - (B) 2D and 3D AFM images of reduced graphene oxide modified GCE (rGO/GCE), (C) - (D) 2D and 3D AFM images of Pd nanoparticles/reduced graphene oxide modified GCE (Pd/rGO/GCE) and (E) - (F) 2D and 3D AFM images of Cu nanoparticles/Pd nanoparticles/reduced graphene oxide modified GCE (Cu/Pd/rGO/GCE).

temperature by cyclic voltammetry (Fig. 8). Voltammograms (a) and (b) related to ACN solution under Ar bubbling and after addition of CO_2, respectively, at the bare GCE surface and at the potential range of −0.5 to −2.2 V at the scan rate of 100 mV s^{-1}. As shown, no redox peaks are seen under these conditions. Voltammogram (c) shows the response of a bare GCE in the solution containing 1.0 mM 4-nitrobenzyl bromide and in the potential range of −0.50 V to −1.45 V after removing O_2 and voltammogram (d) is related to a bare GCE in the solution containing 1.0 mM 4-nitrobenzyl bromide solution which is saturated with CO_2. As it can be seen, upon bubbling of CO_2, both cathodic peak currents (I) and (II) increased markedly while the anodic peak (III) disappeared. This result indicates that the reduction process of CO_2 in the presence of 4-nitrobenzyl bromide and at the bare GCE surface obeys from an EC' mechanism as discussed in more details below. The standard potential of NO_2 group in CH_3CN solvent [53] is more negative than the standard potential of CO_2 [55]. However, the electrode reaction kinetic of CO_2 at the surface of different electrodes is very slow and therefore its reduction requires a high overpotential. This high overpotential causes the reduction of CO_2 at the surface of different electrodes is performed at more negative potential compared with reduction of NO_2 group.

Constant potential coulometry, CPC, of the 4-nitrobenzyl bromide solution saturated with CO_2 at the potential step of reduction peak (I), voltammogram (d) of Fig. 8, indicates that a charge of 2.04 F mol^{-1} is consumed. Moreover, the spectral characteristics of FTIR, ^1H and ^{13}C NMR of the electrolysis product (Figs. S2–S5) imply the formation of 4-nitrophenylacetate and oxalate as the main and the side products, respectively. These results show that 4-nitrobenzyl bromide is carboxylated at the potential of reduction peak (I) of voltammogram (d).

The electrochemical reduction of simple aromatic halides in the

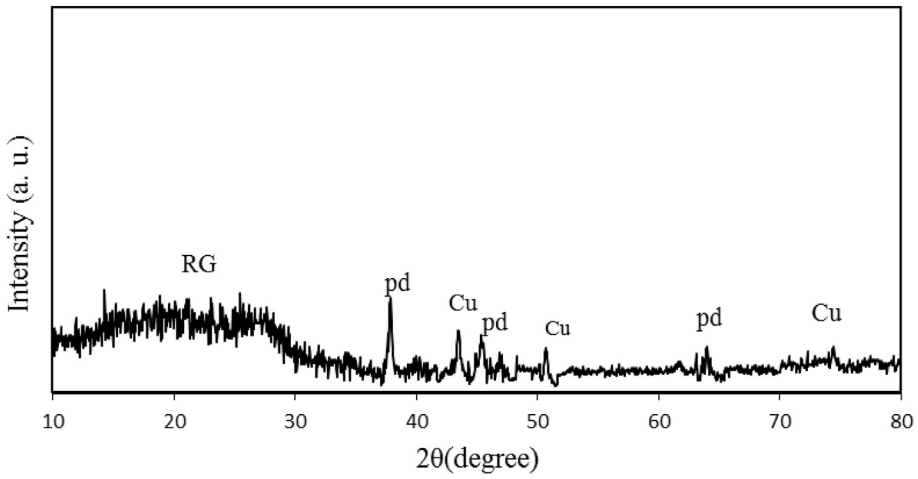

Fig. 3. A) XRD pattern of the Cu nanoparticles/Pd nanoparticles/reduced graphene oxide modified glassy carbon electrode (Cu/Pd/rGO/GCE).

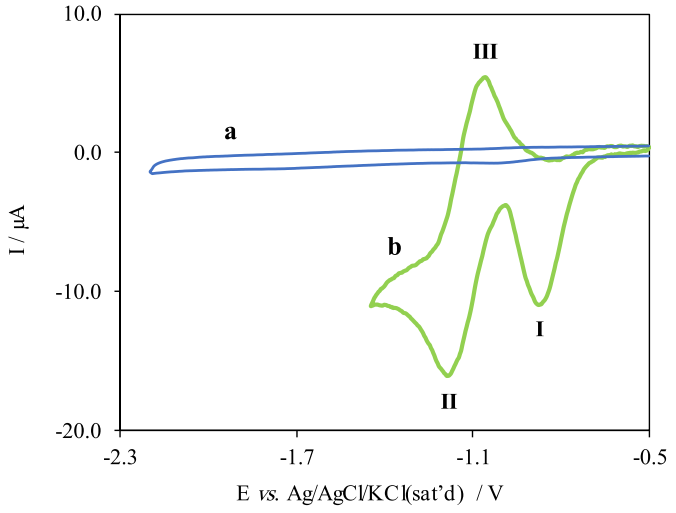

Fig. 4. Cyclic voltammograms of an acetonitrile (0.1 M TBAP) solution after removing O_2 (a) at the bare GCE surface in the potential range of −0.5 V to −2.2 V and (b) as (a) in the presence of 1.0 mM 4-nitrobenzyl bromide in the potential range of −0.5 V to −1.45 V. Potential scan rate: 100 mV s^{-1}.

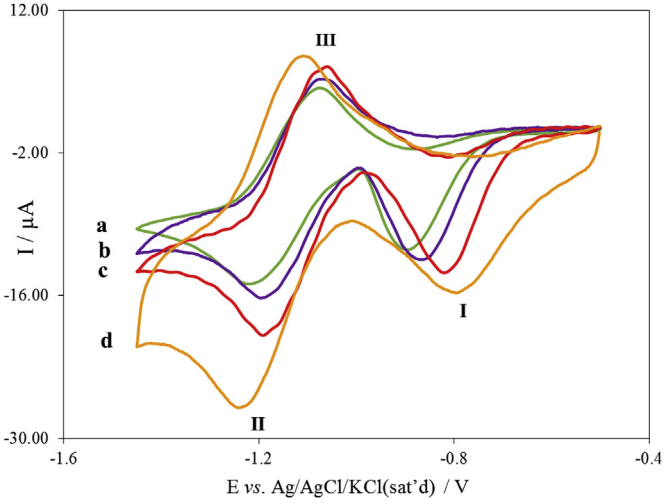

Fig. 5. Cyclic voltammograms of an acetonitrile (0.1 M TBAP) solution containing 1.0 mM 4-nitrobenzyl bromide after removing O_2 (bubbled with Ar gas for 20 min) in the potential range of −0.5 V to −1.45 V at the surface of (a) a bare GCE (b) rGO/GCE, (c) Pd/rGO/GCE and (e) Cu/Pd/rGO/GCE. Potential scan rate: 100 mV s^{-1}.

presence of CO_2 involves a one-electron reduction process which leads to breaking of the carbon-halogen bond [56]. Afterwards, the produced radical, $^{\bullet}CH_2Ar$, takes the second electron to form a carbanion $^{-}CH_2Ar$. As a result, phenyl acetic acid anion, $^{-}O_2CCH_2Ar$, is formed by the nucleophilic attack of the produced carbanion, $^{-}CH_2Ar$, to CO_2 [57]. It is noted that the electrochemical reduction of simple aromatic halides and aromatic halides with electron withdrawing groups (such as nitro group) is different. In other words, when the radical anion is stabilized by electron withdrawing groups, the rate of cleavage is not fast [58]. Thus in Scheme 1A, the reaction rate (b) is greater than the rate of the C-Br bond cleaves in the radical anion shown in reaction (c). However, formation of 1,2-bis(4-nitrophenyl) ethane, $O_2NArCH_2CH_2ArNO_2$, in the absence of CO_2 proves that the reduced form of 4-nitrobenzyl bromide is dimerized instead of taking the second electron [23,54]. This is due to the reduction of the nitro group at less negative potentials, which leads to an intramolecular electron transfer to the carbon-halogen bond [23,54]. The electrocarboxylation of 4-nitrobenzyl bromide at the reduction potential of peak (I), suggests that the process proceeds by a different mechanism. Based on the cyclic voltammetric responses and the spectral characteristics of the product determined through coulometry, which will be discussed later, an EC'C mechanism (Scheme 1A) is proposed for the electrocarboxylation of 4-nitrobenzyl bromide in the presence of CO_2 and at the potential step of reduction peak (I). According to this mechanism, after reduction of 4-nitrobenzyl bromide (Scheme 1A, reaction a), CO_2 is activated by taking one electron from the reduced form of 4-nitrobenzylbromide (Scheme 1A, reaction b). The increase in the reduction current of peak (I), after bubbling of CO_2 (comparison of voltammograms (c) and (d) of Fig. 8), can prove that 4-nitrobenzyl bromide has a catalytic activity for reduction of CO_2. (reactions (a) and (b) of Scheme 1A) [53]. Then, the activated CO_2, $CO_2^{\bullet-}$, reacts with the reduced form of 4-nitrobenzyl bromide, which is a radical anion, (Scheme 1A, reaction c). By the reaction of the radical anions, the carbon-bromide bond cleaves, and the 4-nitrophenylacetate anion is formed (Scheme 1A, reaction c). As seen in Scheme 1A, 4-nitrobenzylbromide is a catalyst with a double role in the electrosynthesis of 4-nitrophenylacetate. The roles include the catalytic reduction of CO_2 by the reduced form of 4-nitrobenzyl bromide (Scheme 1A, reaction b) and the subsequent chemical reaction of

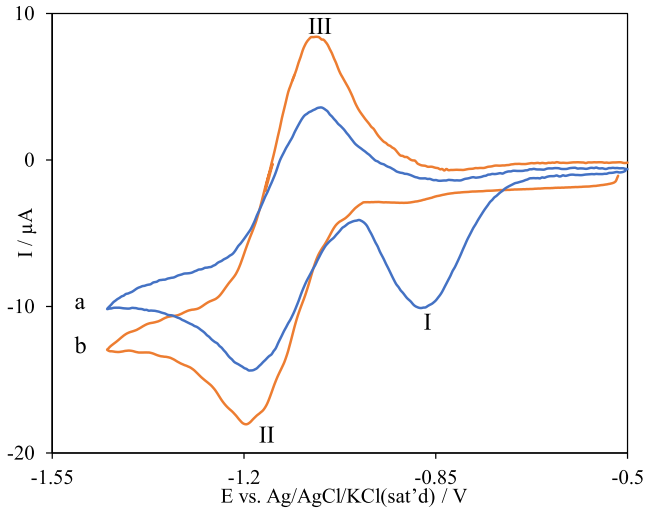

Fig. 6. Cyclic voltammograms of an acetonitrile (0.1 M TBAP) solution containing (a) 1.0 mM 4-nitrobenzyl bromide and (b) 1.0 mM 1,2-bis(4-nitrophenyl) ethane (product of 4-nitrobenzyl bromide electrolysis in the absence of CO_2) after removing O_2 (bubbled with Ar gas for 20 min), in the potential range of −0.5 V to −1.45 V at the surface of a bare GCE. Potential scan rate: 100 mV s^{-1}.

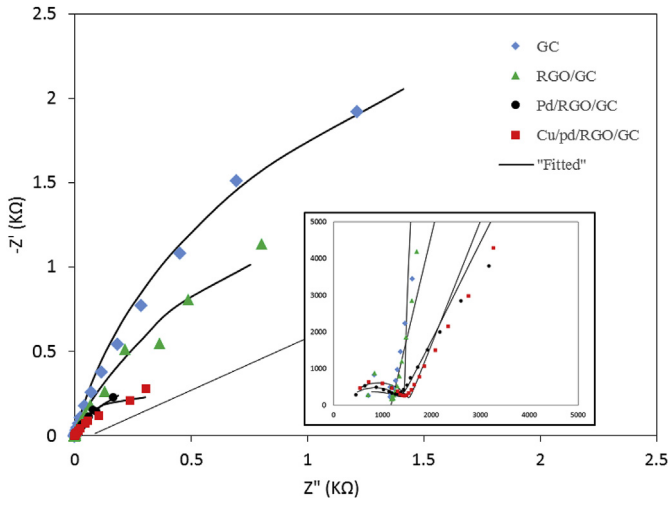

Fig. 7. EIS of acetonitrile solution (0.1 M TBAP) containing 1.0 mM 4-nitrobenzyl bromide at the surface of bare GCE, rGO/GCE, Pd/rGO/GCE and Pd/rGO/GCE.

the reduced form of 4-nitrobenzyl bromide with the produced $CO_2^{\bullet-}$ (Scheme 1A, reaction c). Based on this mechanism, the value of n is expected to be more than one electron corresponding to the reduction reaction (a) of Scheme 1A. In fact, the value of n depends on the number of catalytic cycles (reactions (a) and (b) of Scheme 1A) that occur during the CPC experiment. In other words, the value of n for above catalytic mechanism (EC' mechanism) will be increased, because 4-nitrobenzyl bromide is continuously replenished by the catalytic chemical reaction (b). The extent of this increase will depend on the duration (characteristic time or life time) of the catalytic chemical reaction (b) and the coupled chemical reaction (c) of Scheme 1A. It should be noted that time window of CPC method is very larger than characteristic time of the catalytic chemical reaction (b) or the coupled chemical reaction (c). The n value equal 2 indicates that the catalytic cycle is repeated only one times for each reduced form of 4-nitrobenzyl bromide. This fact,

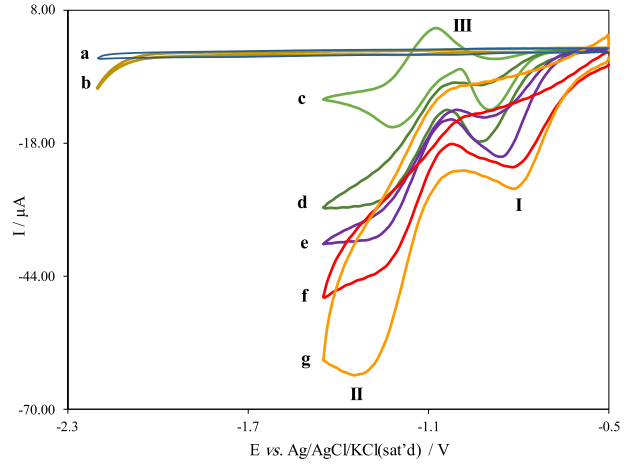

Fig. 8. Cyclic voltammograms of an acetonitrile (0.1 M TBAP) solution after removing O_2 (a) at the bare GCE surface in the potential range of −0.5 V to −2.2 V, (b) as (a) after addition of CO_2, (c) as (a) containing 1.0 mM 4-nitrobenzyl bromide in the potential range of −0.5 V to −1.45 V, (d) as (c) after addition of CO_2. Others voltammograms as (d) at the surface of (e) rGO/GCE, (f) Pd/rGO/GCE and (g) Cu/Pd/rGO/GCE. Potential scan rate: 100 mV s^{-1}.

indicates that the life time of the coupled chemical reaction (c) of Scheme 1A is very short. In other words, by producing a reduced form of 4-nitrobenzyl bromide (reaction (a) of Scheme 1A), the electrocatalytic cycle is performed once and an activated CO_2 is produced. The two species (reduced form of 4-nitrobenzyl bromide and $CO_2^{\bullet-}$) then react with each other rapidly and the electrocatalytic cycle is stopped by the use of the anion radical (reduced form of 4-nitrobenzyl bromide). In this case, the value of n is expected to be 2.

According to the proposed mechanism and the obtained product of CPC at the potential step of peak (I), reduction current of peak (II) of voltammogram (d) is related to the reduction reaction of 4-nitrophenylacetate, $NO_2ArCH_2COO^-$, (Scheme 1B, reaction a′). The significant increase in the reduction current and the decrease in the oxidation current in the presence of CO_2 (comparison of peaks II and III of voltammograms c and d of Fig. 8) demonstrate that the reduced form of 4-nitrophenylacetate, in reduction peak II, also acts as an intermediate in the electrocatalytic reduction of CO_2 (Scheme 1B, reactions a′ and b′). The electrochemical behavior of 4-nitrophenylacetate has been investigated and a quasi-reversible couple has been reported for it [47]. The reduction peak is attributed to the one-electron reduction of the nitro group of $NO_2ArCH_2COO^-$ to yield the respective radical anion, $NO_2^{\bullet-}ArCH_2COO^-$, whereas the anodic peak is attributed to the oxidation of this intermediate to the starting compound, $NO_2ArCH_2COO^-$. As it can be seen in Fig. 8, peaks II and III are in the same region. Therefore, the catalytic effect is related to 4-nitrophenylacetate. Voltammograms (e)-(g) correspond to the catalytic reduction current of CO_2 by 4-nitrophenylacetate at the rGO/GCE (voltammogram e), Pd/rGO/GCE (voltammogram f) and Cu/Pd/rGO/GCE (voltammogram g) surfaces. Comparison of voltammograms (d) and (e) of Fig. 8 indicates that the catalytic reduction current of CO_2 by 4-nitrophenylacetate at the rGo/GCE surface (voltammogram e) is higher than that at the bare GCE surface (voltammogram d). Also, the potential of peak I at the rGO/GCE surface is less negative than that at the bare GCE surface. These results demonstrate that rGO/GCE is a better modified electrode for CO_2 catalytic reduction by 4-nitrophenylacetate. Voltammogram (f) shows that the catalytic reduction current of CO_2 by 4-nitrophenylacetate (peak current I) increase at the Pd/rGO/GCE

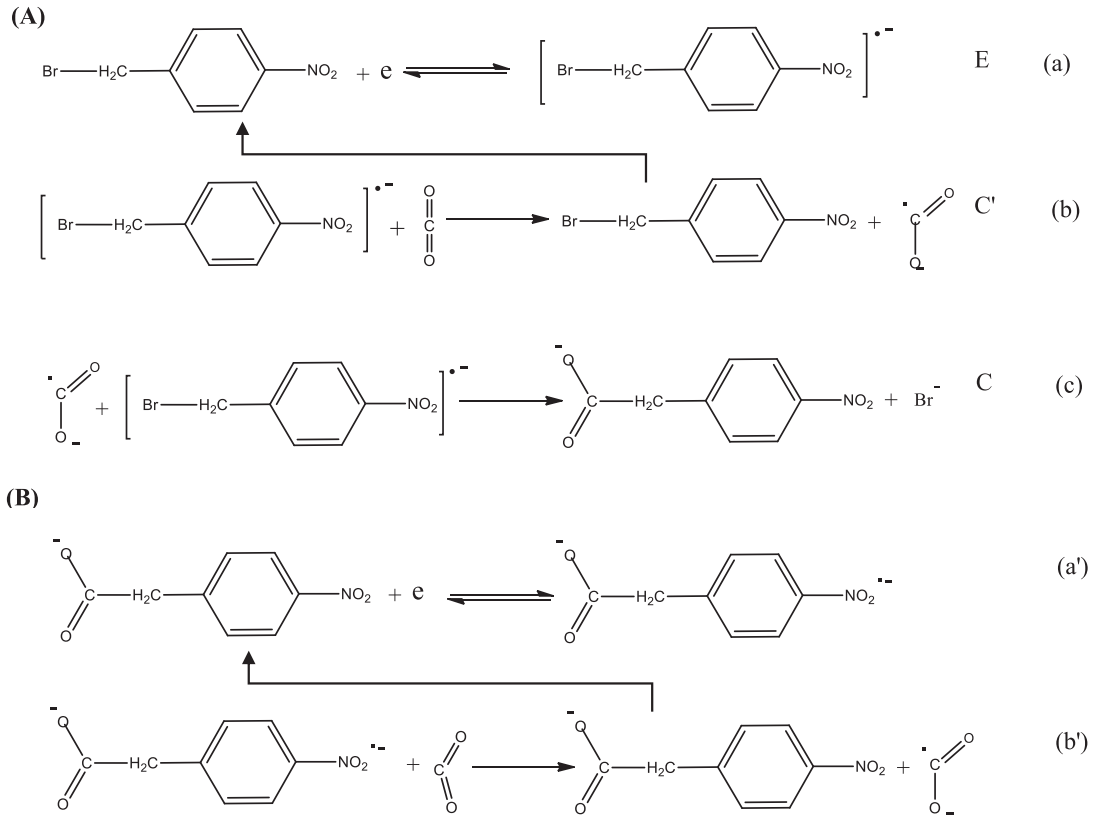

Scheme 1. A) Proposed mechanism corresponding to the catalytic activity of 4-nitrobenzyl bromide for electrocatalytic reduction of CO_2 and its application for synthesis of 4-nitrophenylacetate. B) Electrocatalytic reduction mechanism of CO_2 by 4-nitrophenylacetate

surface compared with a rGO/GCE. Also, the onset potential and reduction peak potential of CO_2 reduction at the Pd/rGO/GCE surface are less negative than the onset potential and reduction peak potential at the rGO/GCE surface. Voltammogram (g) of Fig. 8 demonstrate that the catalytic reduction of CO_2 by 4-nitrophenylacetate has the highest reduction peak current and the less negative peak potential at the Cu/Pd/rGO/GCE surface. Consequently, Cu/Pd/rGO/GCE is the best platform for electrocatalytic reduction of CO_2 by 4-nitrophenylacetate.

Fig. 9 shows the cyclic voltammograms of ACN solution containing 1.0 mM 4-nitrobenzyl bromide (voltammogram a) and ACN solution containing 1.0 mM tetrabutylammonium 4-nitrophenylacetate (product of 4-nitrobenzyl bromide electrolysis in presence of CO_2) (voltammogram b) after removing O_2 at bare GCE surface. Also, voltammogram (c) of Fig. 9 shows the response of CO_2-saturated ACN solution containing 1.0 mM tetrabutylammonium 4-nitrophenylacetate at a bare GCE surface. Comparison of voltammograms of Fig. 9 with voltammograms of Fig. 8 also confirms the mechanism proposed in Scheme 1. Furthermore, consecutive cycles of Cu/pd/rGO/GC electrode in ACN solution (0.1 M TBAP) containing 4-nitrobenzyl bromide and CO_2 are recorded (not shown). The results indicate that the Cu/pd/rGO/GC electrode has a good stability.

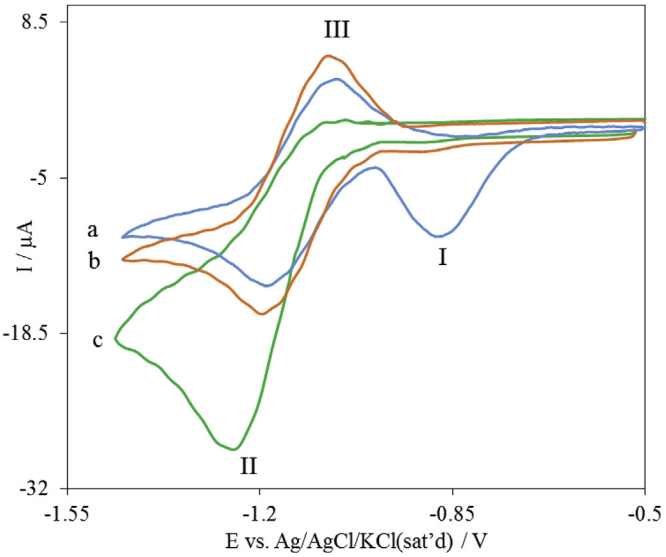

Fig. 9. Cyclic voltammograms of an acetonitrile (0.1 M TBAP) solution containing (a) 1.0 mM 4-nitrobenzyl bromide and (b) 1.0 mM tetrabutylammonium 4-nitrophenylacetate (product of 4-nitrobenzyl bromide electrolysis in the presence of CO_2) after removing O_2 in the potential range of −0.5 V to −1.45 V at the surface of a bare GCE. (c) as (b) after addition of CO_2. Potential scan rate: 100 mV s^{-1}.

4. Conclusion

The results of this research demonstrate that 4-nitrobenzyl bromide can be electrocarboxylated by CO_2 at the Cu/Pd/rGO/GCE surface at the potential of −0.80 V versus Ag/AgCl/KCl (sat'd). Based on cyclic voltammetric data and spectral characteristics of the coulometric product, it is proved that the reduced form of 4-nitrobenzyl bromide has a dual activity in the presence of CO_2.

These activities include electron transfer to CO_2 to form $CO_2^{\bullet-}$ and then a chemical reaction with the produced $CO_2^{\bullet-}$ to produce 4-nitrophenylacetate. An EC'C mechanism is proposed for the whole process. Based on this mechanism, 4-nitrobenzyl bromide can be used for electrocatalytic reduction of CO_2 and as an initial substrate for electrosynthesis of 4-nitrophenylacetate. Finally, it is shown that the modified electrode of Cu/Pd/rGO/GCE provide synergistic effect which causes to decrease the reduction overpotential of CO_2 by 4-nitrobenzyl bromide.

Declaration of competing interest

The authors declare that they have no known competing financial interests or personal relationships that could have appeared to influence the work reported in this paper.

CRediT authorship contribution statement

Safoora Mohammadzadeh: Writing - original draft, Investigation, Data curation. **Hamid R. Zare:** Supervision, Conceptualization, Writing - review & editing, Validation. **Hossein Khoshro:** Conceptualization, Writing - review & editing, Validation. **Kobra Ghobadi:** Writing - original draft, Investigation, Data curation. **Ali Benvidi:** Software.

Acknowledgment

The authors are grateful for the support of the Iran National Science Foundation, INSF, Iran, under Grant No. 96004700.

Appendix A. Supplementary data

Supplementary data to this article can be found online at https://doi.org/10.1016/j.electacta.2020.136483.

References

[1] P.V. Hobbs, Introduction to Atmospheric Chemistry, Cambridge University Press, 2000.
[2] T. Kuc, K. Rozanski, M. Zimnoch, J.M. Necki, A. Korus, Anthropogenic emissions of CO_2 and CH_4 in an urban environment, Appl. Energy 75 (2003) 193–203.
[3] D.J. Darensbourg, Making plastics from carbon dioxide: salen metal complexes as catalysts for the production of polycarbonates from epoxides and CO_2, Chem. Rev. 107 (2007) 2388–2410.
[4] L. Quinn, C.L. Jones, Carbon Dioxide, Reinhold Publishing Corporation, New York, 1936.
[5] C. Bamberger, P.R. Robinson, The electrochemical reactions of copper(II) and copper(I) chloride in n, n-dimethylformamide, Inorg. Chim. Acta. 42 (1980) 133–137.
[6] C. Willis, A. Boyd, Excitation in the radiation chemistry of inorganic gases, J. Radiat. Phys. Chem. 8 (1976) 71–111.
[7] A. Call, M. Cibian, K. Yamamoto, T. Nakazono, K. Yamauchi, K. Sakai, Highly efficient and selective photocatalytic CO_2 reduction to CO in water by a cobalt porphyrin molecular catalyst, ACS Catal. 9 (2019) 4867–4874.
[8] H.S. Jee, N. Nishio, S. Nagai, CH_4 production from H_2 and CO_2 byMethanobacterium thermoautotrophicum cells fixed on hollow fibers, Biotechnol. Lett. 10 (1988) 243–248.
[9] D. Mandler, I. Willner, Photochemical fixation of carbon dioxide: enzymic photosynthesis of malic, aspartic, isocitric, and formic acids in artificial media, J. Chem. Soc. Perkin Trans. 2 (1988) 997–1003.
[10] B.A. Parkinson, P.F. Weaver, Photoelectrochemical pumping of enzymatic CO_2 reduction, Nature 309 (1984) 148.
[11] J. Yuan, Y. Wang, Photoelectrochemical reduction of carbon dioxide to methanol at CuS/CuO/$CuInS_2$ thin film photocathodes, J. Electrochem. Soc. 164 (2017) E475–E479.
[12] I. Taniguchi, B. Aurian-Blajeni, B. Jom, The reduction of carbon dioxide at illuminated p-type semiconductor electrodes in nonaqueous media, Electrochim. Acta 29 (1984) 923–932.
[13] S. Sen, D. Liu, G.T.R. Palmore, Electrochemical reduction of CO_2 at copper nanofoams, ACS Catal. 4 (2014) 3091–3095.
[14] K. Sugimura, S. Kuwabata, H. Yoneyama, Electrochemical fixation of carbon dioxide in oxoglutaric acid using an enzyme as an electrocatalyst, J. Am. Chem. Soc. 111 (1989) 2361–2362.
[15] J. Wu, F.G. Risalvato, P.P. Sharma, P.J. Pellechia, F.-S. Ke, D. Zhou, Electrochemical reduction of carbon dioxide II. Design, assembly, and performance of low temperature full electrochemical cells, J. Electrochem. Soc. 160 (2013) F953–F957.
[16] G.A. Olah, A. Goeppert, G.S. Prakash, Chemical recycling of carbon dioxide to methanol and dimethyl ether: from greenhouse gas to renewable, environmentally carbon neutral fuels and synthetic hydrocarbons, J. Org. Chem. 74 (2008) 487–498.
[17] E.M. Nichols, C.J. Chang, Urea-Based Multipoint hydrogen-bond donor additive promotes electrochemical CO_2 reduction catalyzed by nickel cyclam, Organometallics 38 (2018) 1213–1218.
[18] K. Ghobadi, H.R. Zare, H. Khoshro, A.A. Jafari, Excellent electrocatalytic activity of benzil for direct reduction of CO_2 as well as indirect reduction of pyridine: a kinetic view of the electrocarboxylation process, J. Energ. Chem. 26 (2017) 569–573.
[19] C. Amatore, A. Jutand, Activation of carbon dioxide by electron transfer and transition metals. Mechanism of nickel-catalyzed electrocarboxylation of aromatic halides, J. Am. Chem. Soc. 113 (1991) 2819–2825.
[20] S. Derien, J.C. Clinet, E. Dunach, J. Perichon, Activation of carbon dioxide: nickel-catalyzed electrochemical carboxylation of diynes, J. Org. Chem. 58 (1993) 2578–2588.
[21] J. Canales, J. Ramirez, G. Estiu, J. Costamagna, Bis-bipyridine hexa-aza-macrocycle complexes of zinc (II) and nickel (II) and the catalytic reduction of carbon dioxide, Polyhedron 19 (2000) 2373–2381.
[22] S. Rezaee, S. Shahrokhian, M.K. Amini, Nanocomposite with promoted electrocatalytic behavior based on bimetallic Pd–Ni nanoparticles, manganese dioxide, and reduced graphene oxide for efficient electrooxidation of ethanol, J. Phys. Chem. C 122 (2018) 9783–9794.
[23] L. Álvarez-Griera, I. Gallardo, G. Guirado, Estimation of nitrobenzyl radicals reduction potential using spectro-electrochemical techniques, Electrochim. Acta 54 (2009) 5098–5108.
[24] J. Bays, S. Blumer, S. Baral-Tosh, D. Behar, P. Netav, Intramolecular electron transfer and dehalogenation of nitroaromatic anion radicals, J. Am. Chem. Soc. 105 (1983) 320–324.
[25] Y. Xia, Z.Y. Yang, P. Xia, K.F. Bastow, Y. Nakanishi, P. Nampoothiri, E. Hamel, A. Brossi, K.H. Lee, Antitumor agents. Part 226: synthesis and cytotoxicity of 2-phenyl-4-quinolone acetic acids and their esters, Bioorg. Med. Chem. Lett 13 (2003) 2891–2893.
[26] T. Li, S. Hilton, K.D. Janda, The potential application of catalytic antibodies to protecting group removal: catalytic antibodies with broad substrate tolerance, J. Am. Chem. Soc. 117 (1995) 2123–2127.
[27] E. Yoo, T. Okata, T. Akita, M. Kohyama, J. Nakamura, I. Honma, Enhanced electrocatalytic activity of Pt subnanoclusters on graphene nanosheet surface, Nano Lett. 9 (2009) 2255–2259.
[28] E. Antolini, Graphene as a new carbon support for low-temperature fuel cell catalysts, Appl. Catal., B 123 (2012) 52–68.
[29] S. Shahrokhian, S. Rezaee, Fabrication of trimetallic Pt– Pd– Co porous nanostructures on neduced graphene oxide by galvanic replacement: application to tlectrocatalytic oxidation of ethylene glycol, Electroanalysis 29 (2017) 2591–2601.
[30] O.J. Dada, D. Villaroman, Superior Electronic and delectric properties of corrugated electrochemically reduced graphene over graphene oxide papers, J. Electrochem. Soc. 166 (2019) D21–D36.
[31] M. Pumera, A. Ambrosi, A. Bonanni, E.L.K. Chng, H.L. Poh, Graphene for electrochemical sensing and biosensing, Trends Anal. Chem. 29 (2010) 954–965.
[32] L. Chen, Y. Tang, K. Wang, C. Liu, S. Luo, Direct electrodeposition of reduced graphene oxide on glassy carbon electrode and its electrochemical application, Electrochem. Commun. 13 (2011) 133–137.
[33] J. Kauppila, P. Kunnas, P. Damlin, A. Viinikanoja, C. Kvarnström, Electrochemical reduction of graphene oxide films in aqueous and organic solutions, Electrochim. Acta 89 (2013) 84–89.
[34] H. Teymourian, A. Salimi, S. Khezrian, Fe_3O_4 magnetic nanoparticles/reduced graphene oxide nanosheets as a novel electrochemical and bioeletrochemical sensing platform, Biosens. Bioelectron. 49 (2013) 1–8.
[35] Ö.A. Yokuş, F. Kardaş, O. Akyıldırım, T. Eren, N. Atar, M.L. Yola, Sensitive voltammetric sensor based on polyoxometalate/reduced graphene oxide nanomaterial: application to the simultaneous determination of l-tyrosine and l-tryptophan, Sensor. Actuator. B Chem. 233 (2016) 47–54.
[36] L.P. Mei, J.J. Feng, L. Wu, J.Y. Zhou, J.R. Chen, A.J. Wang, Novel phenol biosensor based on laccase immobilized on reduced graphene oxide supported palladium–copper alloyed nanocages, Biosens. Bioelectron. 74 (2015) 347–352.
[37] Y. Zhang, J. Zhang, H. Wu, S. Guo, J. Zhang, Glass carbon electrode modified with horseradish peroxidase immobilized on partially reduced graphene oxide for detecting phenolic compounds, J. Electroanal. Chem. 681 (2012) 49–55.
[38] S. Guo, D. Wen, Y. Zhai, S. Dong, E. Wang, Platinum nanoparticle ensemble-on-graphene hybrid nanosheet: one-pot, rapid synthesis, and used as new electrode material for electrochemical sensing, ACS Nano 4 (2010) 3959–3968.
[39] Z. Yao, M. Zhu, F. Jiang, Y. Du, C. Wang, P. Yang, Highly efficient electrocatalytic performance based on Pt nanoflowers modified reduced graphene oxide/carbon cloth electrode, J. Mater. Chem. 22 (2012) 13707–13713.
[40] X. Zhang, X. Wang, L. Le, A. Ma, S. Lin, A Pd/PW12/RGO composite catalyst prepared by electro-codeposition for formic acid electro-oxidation, J. Electrochem. Soc. 163 (2016) F71–F78.

[41] I. Cabria, M. López, J. Alonso, J. heoretical study of the transition from planar to three-dimensional structures of palladium clusters supported on graphene, Phys. Rev. B 81 (2010), 035403.
[42] P. Khomyakov, G. Giovannetti, P. Rusu, G.V. Brocks, J. Van den Brink, P.J. Kelly, First-principles study of the interaction and charge transfer between graphene and metals, Phys. Rev. B 79 (2009) 195425.
[43] Q. Wang, J. Che, Origins of distinctly different behaviors of Pd and Pt contacts on graphene, Phys. Rev. Lett. 103 (2009), 066802.
[44] X. Chen, G. Wu, J. Chen, X. Chen, Z. Xie, X. Wang, Synthesis of "clean" and well-dispersive Pd nanoparticles with excellent electrocatalytic property on graphene oxide, J. Am. Chem. Soc. 133 (2011) 3693–3695.
[45] C. Liu, H. Zhang, Y. Tang, S. Luo, Controllable growth of graphene/Cu composite and its nanoarchitecture-dependent electrocatalytic activity to hydrazine oxidation, J. Mater. Chem. A 2 (2014) 4580–4587.
[46] A. Inesi, L. Rampazzo, A. Zeppa, Polarographic and voltammetric reduction of some aliphatic α-bromoesters, J. Electroanal. Chem. 122 (1981) 246.
[47] V. Ramírez-Delgado, A. Méndez-Albores, A. Galano, F.J. González, The spontaneous decarboxylation of strong carboxylic acid– carboxylate mixtures and the use of carbon surfaces to trap the released free radicals, Electrochim. Acta 245 (2017) 472–481.
[48] S. William, J. Hummers, R.E. Offeman, Preparation of graphitic oxide, J. Am. Chem. Soc. 80 (1958) 1339.
[49] J. Yang, S. Gunasekaran, Electrochemically reduced graphene oxide sheets for use in high performance supercapacitors, Carbon 51 (2013) 36–44.
[50] S. Thiagarajan, R.F. Yang, S.M. Chen, Palladium nanoparticles modified electrode for the selective detection of catecholamine neurotransmitters in presence of ascorbic acid, Bioelectrochemistry 75 (2009) 163–169.
[51] K.C. Lin, Y.C. Lin, S.M. Chen, A highly sensitive nonenzymatic glucose sensor based on multi-walled carbon nanotubes decorated with nickel and copper nanoparticles, Electrochim. Acta 96 (2013) 164–172.
[52] J.-J. Lv, S.-S. Li, A.-J. Wang, L.-P. Mei, J.-J. Feng, J.-R. Chen, Z. Chen, One-pot synthesis of monodisperse palladium–copper nanocrystals supported on reduced graphene oxide nanosheets with improved catalytic activity and methanol tolerance for oxygen reduction reaction, J. Power Sources 269 (2014) 104–110.
[53] A.J. Bard, L.R. Faulkner, J. Leddy, C.G. Zoski, Electrochemical Methods: Fundamentals and Applications, Wiley, New York, 2001.
[54] H. Burrows, E.M. Kosower, Optical spectra and reactivities of radical anions of 4-nitrobenzyl compounds produced by pulse radiolysis of acetonitrile solutions, J. Phys. Chem. 78 (1974) 112–117.
[55] M.L. Pegis, J.A.S. Roberts, D.J. Wasylenko, E.A. Mader, A.M. Appel, J.M. Mayer, Standard reduction potentials for oxygen and carbon dioxide couples in acetonitrile and N,N-dimethylformamide, Inorg. Chem. 54 (2015) 11883–11888.
[56] C. Amatore, A. Jutand, F. Khalil, M.F. Nielsen, Carbon dioxide as a C1 building block. Mechanism of palladium-catalyzed carboxylation of aromatic halides, J. Am. Chem. Soc. 114 (1992) 7076–7085.
[57] H. Khoshro, H.R. Zare, A. Gorji, M. Namazian, A.A. Jafari, R. Vafazadeh, The effect of electronic structure on electrocatalytic behaviors of cobalt Schiff base complexes: electrosynthesis of 2-phenylacetic acid using carbon dioxide, J. Electroanal. Chem. 732 (2014) 117–121.
[58] C.L. Scortichini, S.J. Babinec, The effect of cathode composition on the efficiency of electrocarboxylation of aromatic halides, J. Electroanal. Chem. 379 (1994) 111–120.